J Polym Res (2017) 24: 148
DOI 10.1007/s10965-017-1312-6

ORIGINAL PAPER

Effect of processing method on microstructure, electrical conductivity and electromagnetic wave interference (EMI) shielding performance of carbon nanofiber filled thermoplastic polyurethane composites

Alper Kasgoz[1] · **Mehmet Korkmaz**[2] · **Mine Begum Alanalp**[3] · **Ali Durmus**[3]

Received: 20 February 2017 / Accepted: 20 August 2017 / Published online: 28 August 2017

Abstract In this study, effect of processing method on microstructure formation and related electrical conductivity and electromagnetic interference shielding effectiveness of carbon nanofiber (CNF) filled thermoplastic polyurethane (TPU) composites, prepared via three different processing techniques; (i) melt compounding (MC) in a twin screw extruder, (ii) simple solution mixing (SM) on a magnetic stirrer, and (iii) solution mixing with sonication (SM-U) were investigated. It was found that the electrical conductivity values of samples decreased in the order of SM > SM-U > MC for a particular amount of CNF. The electromagnetic test results showed that the samples prepared with SM and SM-U methods yielded higher total shielding effectiveness (SE_T) values than those prepared with MC. SE_T values of samples including of 20 phr of CNF prepared with MC, SM-U and SM methods were varied in the range of 10–30 dB, 20–60 dB and 20–80 dB, respectively within a frequency range of 1–12 GHz.

Keywords Composites · Electron microscopy · Polyurethanes · Processing · Structure-property relations

✉ Ali Durmus
durmus@istanbul.edu.tr

[1] Faculty of Engineering, Polymer Engineering Department, Yalova University, 77100 Yalova, Turkey

[2] Faculty of Engineering, Electric and Electronic Engineering Department, Selcuk University, 42075 Konya, Turkey

[3] Faculty of Engineering, Department of Chemical Engineering, Istanbul University, 34320, Avcılar, Istanbul, Turkey

Introduction

Electromagnetic interference (EMI) is defined as the disruptive electromagnetic radiation which can affect electrical equipment and living spaces. In recent years, many studies have been published on harmful and possible carcinogenic effects of electromagnetic waves [1–3] for humans as well as disruptive effects for sensitive electronic equipment in case of long-term exposure [4–6]. The most commonly used technique to avoid disruptive effects of EMI is isolation of sensitive circuits or living spaces simply by using of electromagnetic shielding materials which do not allow propagation of electromagnetic waves.

Although conductive materials such as metallic coatings, foils or sheets have been used as traditional electromagnetic shielding material, conductive polymer composites (CPCs) filled with metal particles or various types of carbon materials have attracted great interest due to their some manufacturing and processing advantages [7, 8]. Utilization of carbon fillers into a CPC composition has been particularly preferred in scientific and industrial applications for last decades due to several technical advantages such as requirement of low filler amount, low filler cost, and ease of processing and preparation of low density composites [9, 10]. Using of different carbon forms; graphite and/or expanded graphite [11, 12], carbon nanofiber (CNF) [9], single or multiwall carbon nanotubes (SWCNT, MWCNT) [13, 14], and graphene nano sheets [15] have been extensively studied for preparation of CPCs for EMI shielding applications. Microstructural and physical properties and shielding effectiveness of CPCs prepared with different types of carbon fillers were characterized and compared [9, 16]. Al-Saleh et al. prepared MWCNT, CNF, and high structure carbon black (HS-CB) filled acrylonitrile-butadiene-styrene (ABS) composites by solvent casting method and investigated *dc*- and *ac*- conductivity, complex

permittivity, and shielding performances of ABS composites, in detail [9]. They reported that the highest shielding effectiveness, about 50 dB, was obtained with ABS-MWCNT composite having a MWCNT amount of 15 wt% and the thickness of 1.1 mm and the EMI shielding effectiveness, permittivity, and electrical conductivity values of composites decreased in order of MWCNT > CNF > CB for a particular amount of filler. They also concluded that higher aspect ratio and electrical conductivity values of MWCNT yielded higher shielding effectiveness for the ABS-MWCNT composites compared to ABS-CNF and ABS-CB counterparts.

Shielding performance of CPCs mainly depends on the amount and types of carbon fillers. But, some physical and microstructural features of fillers such as surface nature, geometry, and aspect ratio of filler, dispersion level, and agglomeration and orientation issues are also important parameters [17, 18]. Comparing of different processing techniques such as injection molding vs. compression molding [19] and ultrasonic mixing vs. three roll milling [20] and the effects of these techniques on the microstructure and physical properties of CPCs have been studied. Arjmand et al. prepared polystyrene (PS)-MWCNT composites by injection molding and compression molding techniques and determined filler orientation depending on the processing method [19]. They reported that injection molded composites showed lower SE_T, electrical conductivity values, and higher electrical percolation threshold than the compression molded samples because injection molding induced to form more oriented MWCNTs dispersion into polymer matrix and thus reduce the number of physical contact between conductive fillers. Yuen et al. prepared PMMA-MWCNT composites by in-situ and ex-situ methods and compared the electrical resistivity and shielding performance of samples [21]. They reported that PMMA-MWCNT samples prepared with in-situ method showed better adhesion between polymer and fillers which lead to lower resistivity, electrical percolation threshold, and higher SE_T values than the samples prepared with ex-situ process.

When an incident electromagnetic wave (E_I) strike a shielding material, two waves, reflected (E_R) and a transmitted waves (E_T), are formed as shown in Fig. 1. In negligible magnetic interaction conditions, total shielding effectiveness (SE_T) can be defined as logarithmic power ratio of the transmitted and incident waves [22]. SE_T value can be calculated with the Eq. 1 and expressed in decibel unit (dB) [22]. A SE_T value of 20 dB which corresponds to the 99% attenuation of incident electromagnetic wave is generally accepted sufficiently enough in many applications. SE_T also can also be quantified as sum of the contribution of three main shielding mechanisms named "reflection (SE_R)", "absorption (SE_A)" and "multiple reflections (SE_{MR})" [8].

$$SE_T = 10\log\left(\frac{P_{in}}{P_{out}}\right) = SE_A + SE_R + SE_{MR} \quad (1)$$

$$SE_R(dB) = -20\log\left(\frac{\eta_0}{4\eta_s}\right) = 39.5 + \frac{10\log\sigma}{2\pi f\mu} \quad (2)$$

$$SE_A(dB) = 8.7at = 8.7t\sqrt{\pi\sigma f\mu'} \quad \left(\sigma = 2\pi f\varepsilon_0|\varepsilon''|\right) \quad (3)$$

$$SE_{MR}(dB) = 20\log\left(1-e^{-2t/\delta}\right) \quad \left(\delta = 1\Big/\pi f\mu\sigma\right) \quad (4)$$

Reflection based shielding contribution (SE_R) depends on the impedance of domain in which wave is propagating and shielding material. The SE_R is calculated with the Eq. 2 where η_0 is the impedance of domain in which wave is propagating, η_s is the surface impedance, σ is the electrical conductivity (S/m in alternating current), μ_r is the magnetic permeability, defined as $\mu = \mu_0 \times \mu_r$ ($\mu_0 = 4\pi \times 10^{-7}$), ε_0 is the permittivity of vacuum, ε'' is the imaginary part of permittivity of shielding material and f is the frequency (Hz) of incident

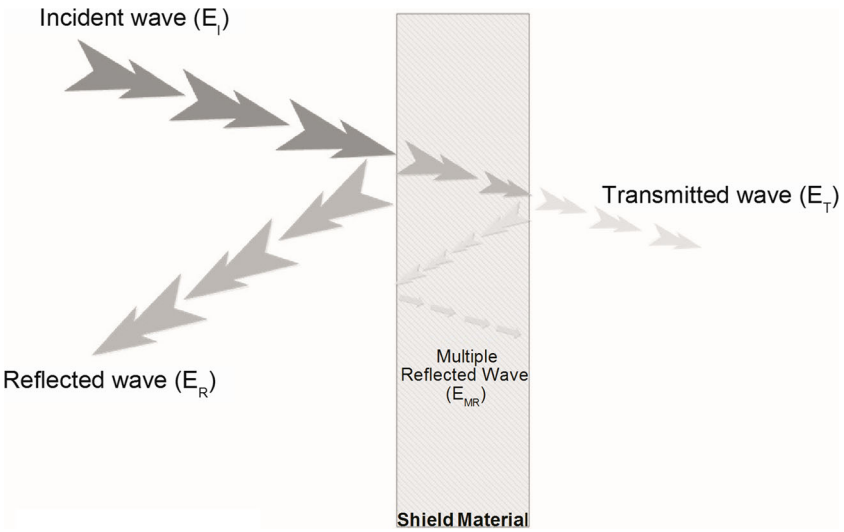

Fig. 1 Schematic representation for different electromagnetic wave shielding mechanisms

EM wave [23]. Reflection of EM wave is related to the interaction between conducting particles into shielding material and electromagnetic wave. Therefore, reflection mechanism is more pronounced in highly conductive materials such as metals, metal coated and/or filled sheets or composites, bulky carbon materials and/or composites, conductive polymers etc.

Equation 3 can be used to calculate the absorption based shielding effectiveness (SE_A) of a material where a is the attenuation constant, t is the thickness (m) [23]. Absorption mechanism is more efficient than reflection mechanism for nano-sized carbon filled composites and magnetic materials [24, 25]. Energy of an incident wave is absorbed by shielding material and converted to heat due to interaction between the electric or magnetic dipole within the shielding materials and electromagnetic wave. Equations 2 and 3 reveal three important conclusions; (i) contributions of reflection and absorption increase with the increasing of conductivity, (ii) contribution of absorption increases while contribution of reflection reduces with the increasing of frequency and (iii) absorption based shielding improves with the increasing thickness of shielding material while reflection based shielding is independent of thickness [26, 27]. Multiple reflections of electromagnetic wave inside a shielding (SEMR) material can also be calculated with Eq. 4 where δ is the skin depth which is a function of frequency. In many cases, the contribution of SE_{MR} to the SE_T is relatively small compared to other shielding mechanisms and thus generally ignored [25].

In this study, effect of three different composite preparation routes on the morphological properties, electrical conductivity and EMI shielding effectiveness of thermoplastic polyurethane (TPU)-CNF composites was investigated.

Materials and methods

Materials

A commercial grade TPU (Desmopan® 3380) kindly donated from Bayer and CNF (Pyrograf® PR-24-XT-LHT) were used in this study. An analytical grade tetrahydrofuran (THF) was also used as solvent for TPU. Before composite preparation, TPU and CNF were properly dried in an air-circulating oven to remove moisture.

Composite preparation

Three different processing methods were used to prepare composite samples (i) melt compounding (MC) in a twin screw extruder followed by compression molding, (ii) simple solution mixing (SM) in a magnetic stirrer and (iii) solution mixing with sonication (SM-U) followed by solvent evaporation. Composite films were obtained by following these different processing methods. CNF content into TPU matrix varied between 5 - 20 phr (part of filler per hundred of polymer). Sample notations and compositions are given in Table 1.

In solution mixing method, a proper amount of CNF was dispersed into 30 ml of THF and vigorously stirred onto a magnetic stirrer for 6 h. In another flask, 3 g TPU was also dissolved into 30 ml of THF. Then the CNF suspension was gradually mixed with the TPU solution and this mixture was stirred for 24 h onto a magnetic stirrer with 600 rpm at room condition. The mixture was poured into glass dishes and left at room temperature for 24 h then at 80 °C in an oven for 48 h for solvent evaporation.

In solution mixing assisted with ultrasound method, the same procedure was applied but an ultrasonic horn (Bandelin Sonopuls, HD 2200) was used in both the preparation of CNF suspension for 30 min and the mixing of TPU solution and CNF suspension steps for 120 min.

Melt compounding method was performed in a lab-scale *co*-rotating twin screw extruder (Rondol Micro Lab., D: 10 mm, L/D: 20) configured with intermeshing screws including of 3D of 4 × 60° followed by 2D of 4 × 90° kneading segments. Solid mixture of TPU granules and CNF powder was loaded into extruder. Temperature profile throughout the barrel from feeding zone to die and screw speed were applied as 185–200–200-220-220 °C and 80 rpm, respectively. Extrudates was cooled down to room temperature by passing throughout a water bath then granulated by a chopper. Composite granules then compression molded between Teflon® sheets in a hot press to obtain film and sheet specimens for conductivity measurements and EMI shielding tests. Compression force was applied as 5 tones for 2 min at 200 °C.

Characterization studies

Morphological properties of CNF and composite samples were investigated by a field emission scanning electron microscope (FE-SEM, FEI Quanta FEG 450) operated at 30 kV. Cryo-fractured surfaces of the film samples were directly

Table 1 Sample notation and compositions

Sample	Amount of filler (phr)	Processing method
SM-5	5	Solution mixing without sonication
SM-10	10	
SM-20	20	
SM-U-5	5	Solution mixing with sonication
SM-U-10	10	
SM-U-20	20	
MC-5	5	Melt compounding
MC-10	10	
MC-20	20	

imaged in the electron microscope after a proper sample preparation.

Electrical conductivity of samples were determined by the testing direct current (*dc*) and alternating current (*ac*) conditions. The *dc*-conductivity measurements were carried out according to two probe method by using a multimeter (Keithley 2100/120, $6_{1/2}$-Digit USB Digital Multimeter). The surfaces of specimens directly contacted with electrodes were coated with a conductive silver paste to provide better surface contact. In this system, bulk resistances of samples were measured at room conditions and the corresponding *dc*-conductivity values were determined with the following relationship;

$$\sigma_{dc} = \frac{L}{(RxA)} \tag{5}$$

where L is the sample length (m), A is the cross-sectional area (m^2) and R is the bulk resistivity of sample (ohm). Resistance measurements were performed several times by using three samples for each compositions. It was observed that there was no significant variation in resistance values of samples for a particular composition. Thus, the conductivity values are reported as the average value of five measurements at least. Equation 6 was employed to determine the *ac*-conductivity values of samples;

$$\sigma_{ac} = 2\pi f \varepsilon_0 \varepsilon'' \tag{6}$$

where f is the frequency in Hz, ε_0 is the permittivity of vacuum (8.854×10^{-12}) and ε" is the imaginary part of permittivity. The ε" values of samples were measured by a vector network analyzer (VNA) as described below.

Scattering parameters (S_{11}, S_{12}, S_{21} and S_{22}) of samples were determined with the measurements according to the *co*-axial line method for plane-wave condition. Schematic representation of measurement configuration is seen in Fig. 2, consisting of Keysight Fieldfox N9926A Vector Network Analyzer (VNA), N1500–001 material measurement software and coaxial airline (85055AR03) with the inner and outer diameter of 3 mm and 7 mm, respectively. Full two-port calibration was performed to neglect any loss due to sample holder and other equipment's by Keysight type N mechanical calibration kits (85518A and 85519A). Three different samples were tested, at least for each composition within the frequency range of 1–12 GHz with an interference bandwidth (IFBW) of 1000 Hz. Complex permittivity (ε^*) values of samples have been calculated by using the experimental scattering parameters according to the Nicolson–Ross–Weir (NRW) algorithm. Outer and inner diameters and thickness values of an o-ring shape test specimen were about 7 mm, 3 mm, and 1 mm, respectively. Correction function of material measurement software was also used to correct errors arising from air gap between the sample and *co*-axial airline.

Results and discussion

Microstructure and morphology

Figure 3a and b show a cocoon-like CNF bundle and nano fibers, respectively. It can be seen that the average size of CNF bundle is in the range of 35–60 μm while an average fiber diameter is about 120 nm. Although the fiber length cannot be precisely determined from Fig. 3b, it was declared as 50–200 μm by the manufacturer.

Figure 4 represents SEM micrographs of SM-20 [(a) and (b)], SM-U-20 [(c) and (d)], and MC-20 [(e) and (f)] samples at different magnifications. Figures given on the left show the cross-sectional and topological appearances and thicknesses of composite films while the other images demonstrate the microstructural features of composites, more precisely. It was found that the thicknesses of composite films were about 220 μm for SM-20 and SM-U-20 and 100 μm for MC-20 samples. It can be easily noticed that the SM-20 sample exhibits very rough topology on both cross-sectional and planar surfaces of film. On the other hand, compression molded film yielded relatively smooth planar surface, due to the processing conditions, as expected. Roughness on the top surfaces of films increases in the order of MC-20 < SM-U-20 < SM-20. It can also be seen that the SM-20 and SM-U-20 samples showed highly porous structure compared to the MC-20. This was possibly due to the effect of solvent evaporation on the microstructure formation. Large holes or voids are not observed around the fibers as seen in Fig. 4b, d and f which indicate that the interfacial interaction between polymer phase and fibers was sufficiently strong because of the highly polar nature of TPU.

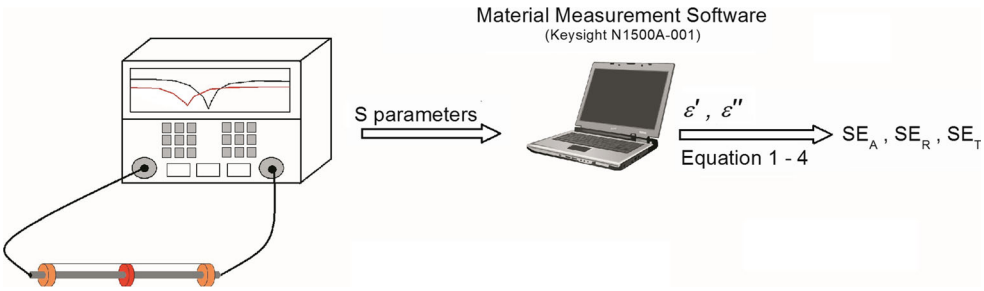

Fig. 2 Schematic representation for the measurement and calculation method of electromagnetic parameters

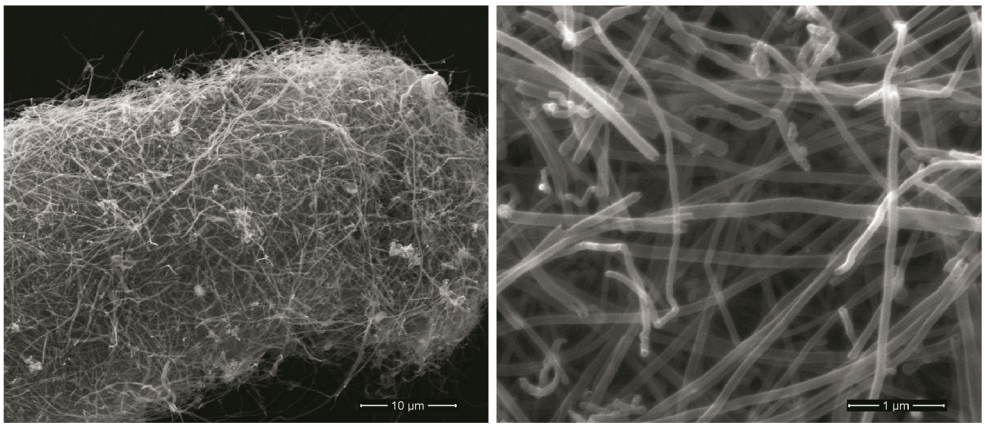

Fig. 3 SEM images of CNF

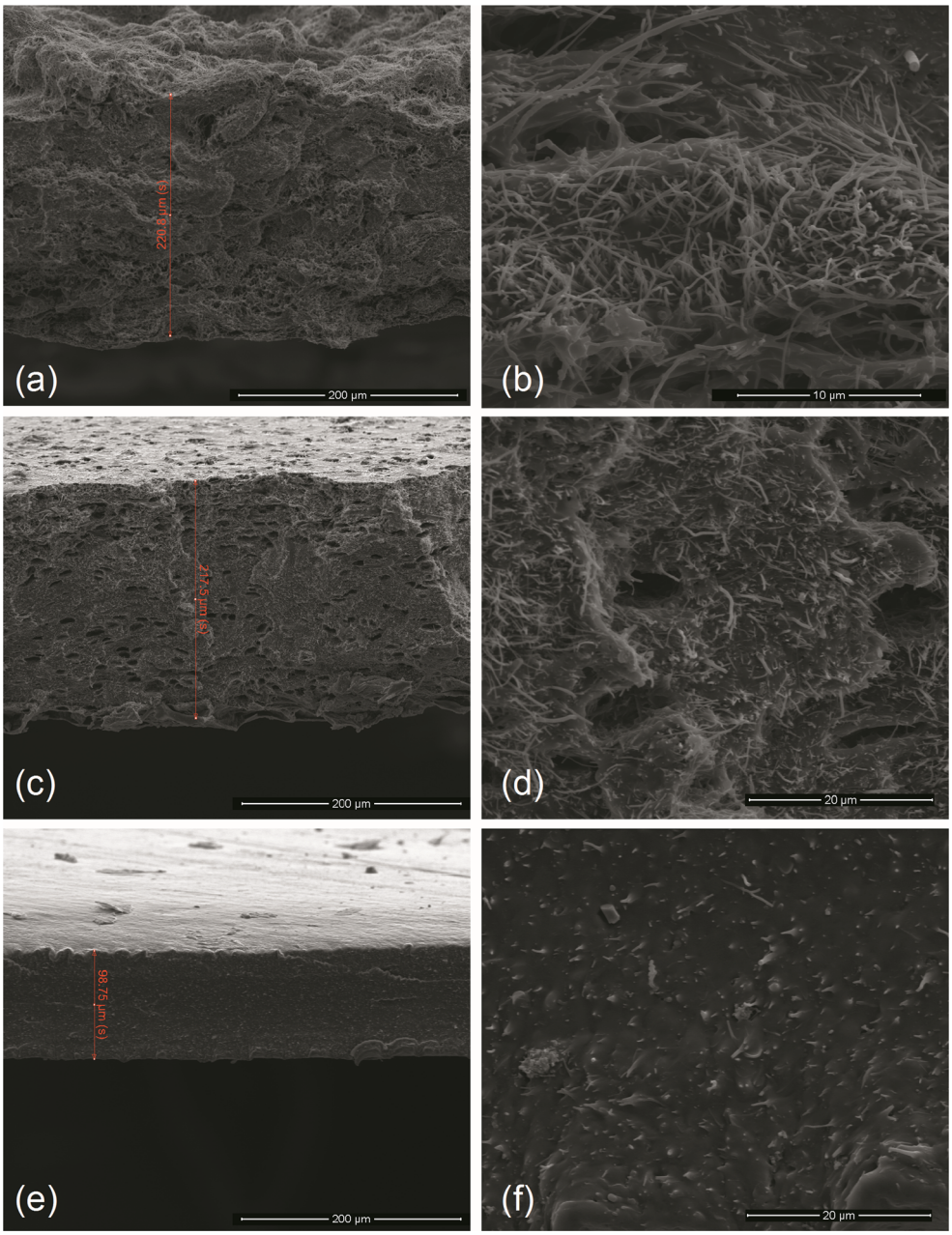

Fig. 4 SEM images of TPU-CNF composite films containing 20 phr of filler prepared with different processing methods (**a** and **b**) SM, (**c** and **d**) SM-U, and (**e** and **f**) MC

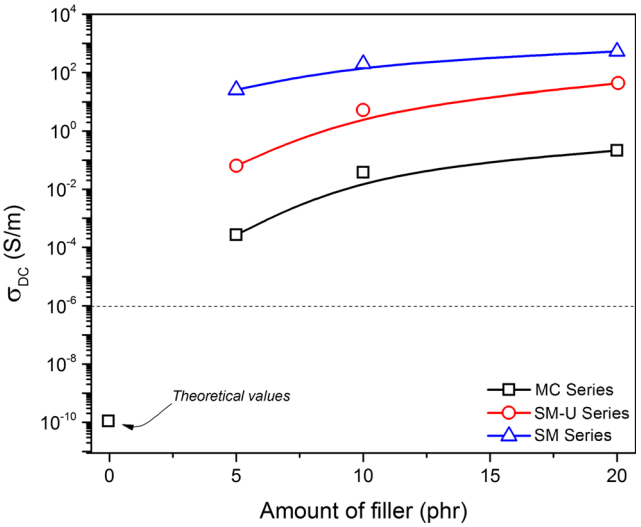

Fig. 5 Dependence of *dc*-conductivity values of samples on the amount of CNF and processing method

On the other hand, dispersion of nano fibers and microstructural properties of samples changes significantly depending on the processing methods. By comparing the microstructural images given in Fig. 4b, d, and f, it can be seen that the CNF bundles were dispersed more homogenously into TPU structure by melt compounding and solution mixing with sonication methods than the simple solution mixing one. On the other hand, it can be concluded that extrusion and ultrasonic mixing methods were not only disentangled CNF bundles and dispersed more uniformly but also broke nano fibers and caused to form shorter fibers having lower aspect ratio ($A_f = L/d$) which can be defined as the ratio of fiber length (L) to its thickness or diameter (d) and generally considered as the most important parameter for electrical conductivity and mechanical properties of composites. SEM observations also implied that both dispersion and fiber breaking were more pronounced in melt compounded composites than SM-U counterparts. Based on the microstructural observations, it can be concluded that the aspect ratio (A_f) values of CNFs were varied significantly depending on the processing technique. It could be assumed that the A_f values of sample series prepared with different methods decreased in the order of SM > SM-U > MC.

Electrical conductivity

Dependence of *dc*-conductivity values of samples on the amount of CNF and processing method are given in Fig. 5. In this figure, *dc*-conductivity of neat TPU was accepted as the theoretical value declared by the manufacturer due to bulk resistance of TPU was much higher than the measurement limits of multimeter. It can be seen in this figure that the *dc*-conductivity of TPU-CNF composites readily increased with the increasing amount of filler, as expected. Semi-log "conductivity (σ)-amount of filler (ϕ)" relationship of CPC generally yields characteristic sigmoidal curves. The transition zone from low conductivity ($<10^{-10}$ S/m) plateau to high conductivity one in these curves is generally accepted as percolation threshold which can be defined as the minimum amount of filler to form a continuous and conductive pathway throughout the sample. In Fig. 5, it is difficult to distinguish the effect of processing method on the percolation. But, it could also be obviously inferred that all series of samples showed a percolation threshold below 5 phr of CNF. Samples prepared with various processing methods exhibited different *dc*-conductivity values at the CNF amount of 5 phr. It was also found that *dc*-conductivity of samples prepared with different methods decreased in the order of SM > SM-U > MC at a particular loading amount of CNF. This relationship can be explained by variation in A_f, filler dispersion, number of conductive pathways and related microstructural features of samples depending on the processing method as mentioned in the previous part. It can be concluded that higher *dc*-conductivity values of samples prepared with SM method originated from higher A_f values of these samples. It can be assumed that the longer fibers form more connection points and conductive pathway throughout the bulk structure of composite.

Figure 6 shows dependence of *ac*-conductivity values of samples on the frequency and compositional parameters. It

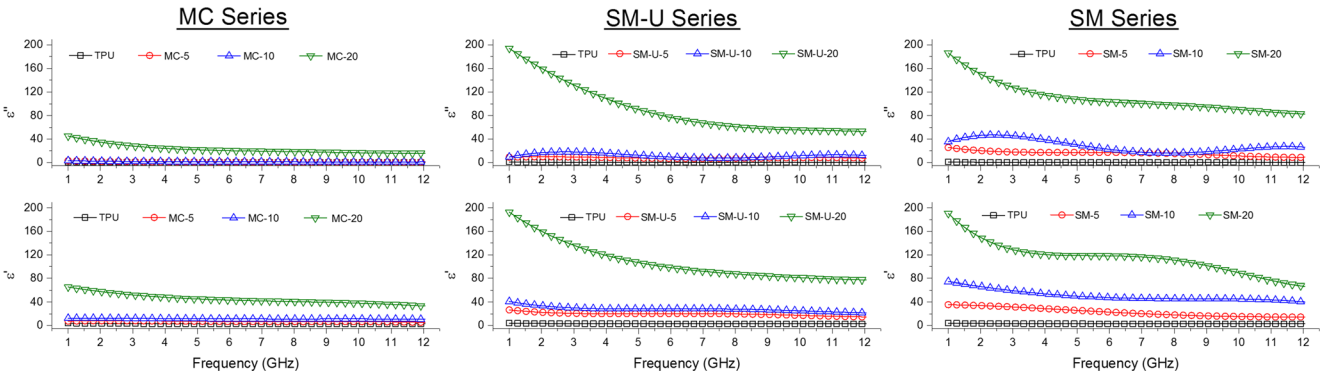

Fig. 6 Dependence of *ac*-conductivity values of samples on the composition and processing method within the frequency range of 1–12 GHz

was obtained that the *ac*-conductivity increased with the increasing amount of CNF, as expected and almost all samples showed higher *ac*-conductivity values at high frequency region. This can be explained by improving of hoping capability of electrons depending on frequency increase. Electrons are generally more excited and can easily hop or transfer from a fiber to another one which are get in contact or located sufficiently close to each other, in high frequency region. Relationship between compositional parameters and *ac*-conductivity values of samples are very consistent with the *dc*-conductivity result mentioned before. In Fig. 6, another noteworthy point is a huge gap between the *ac*- and *dc*-conductivity results of neat TPU. It is a well-known fact that the conduction mechanism in a CPC structure is quite different from that occurs in a polymer phase. In *dc*-conductivity conditions (frequency of few Hz), a solid-polymeric material normally shows very high bulk resistance that corresponds to very low conductivity value. But, a doping effect may decrease bulk resistance or increase conductivity of such a polymeric sample. High frequency VNA measurements in *ac*-conductivity tests (scaled in GHz) may act as a physical doping effect on the conductivity of TPU.

By evaluating the *ac*- and *dc*-conductivity values of series of samples, it could be concluded that the relatively high electrical conductivity values (10^1–10^2 S/m) were obtained for the magnetically stirred samples which can also be considered as sufficiently high for EMI shielding applications.

Dielectric properties

Complex permittivity (ε*) and permeability (μ*) values of materials must be investigated to quantify interactions between sample structure and electromagnetic wave. Complex permittivity (ε*) value reflects the interactions between sample and electrical component of EM wave while the complex permeability (μ*) refers to such relationship between samples and magnetic component of EM wave. Due to complex magnitudes of both parameters, these interactions are generally analyzed by considering the real (ε', μ') and imaginary parts (ε", μ") of parameters. The μ' and μ" values of all samples were supposed to be 1 and 0, respectively because both polymer (TPU) and filler (CNF) phases show no magnetic property.

Figure 7 illustrates dielectric parameters (ε' and ε") of sample series as a function of frequency and amount of filler. It was found that the ε' and ε" values of samples increased with the increasing amount of CNF into composition within the entire frequency range employed. This effect is more pronounced for the SM-U and SM samples. Dielectric parameters also showed a frequency dependent behavior for the samples especially including of relatively higher amount of CNF (15 and 20 phr). It has been reported that the ε' indicates storaged energy within the materials and it is related to polarization

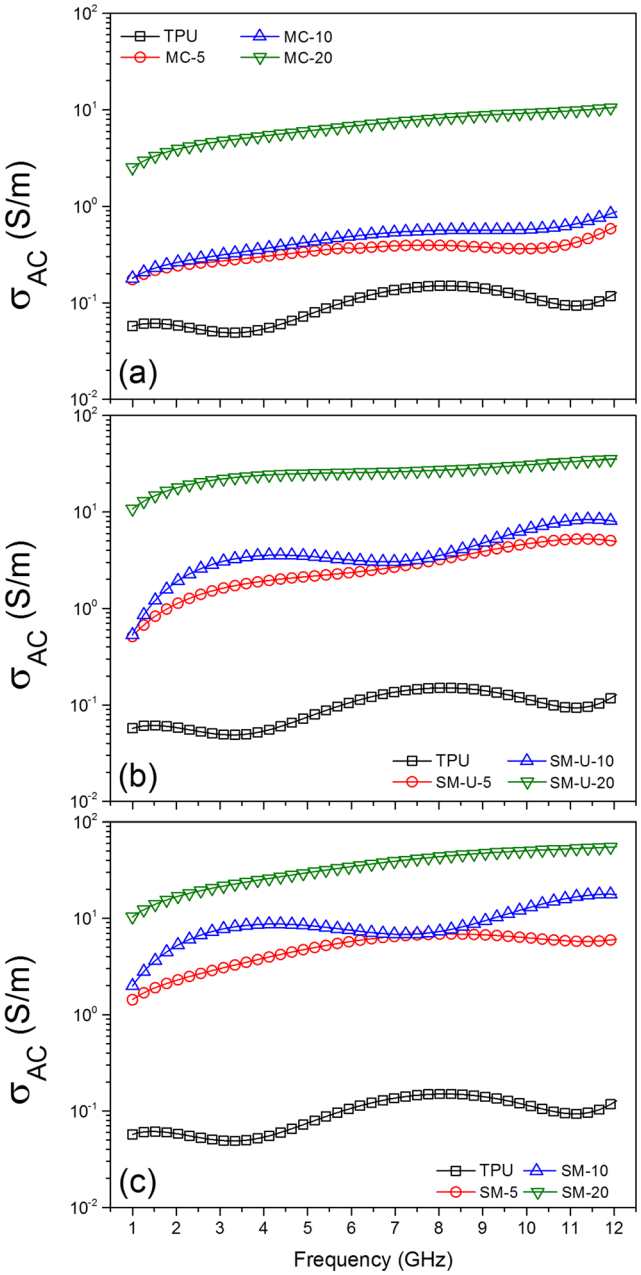

Fig. 7 Dependence of dielectric parameters of samples on the composition and processing method within a frequency range of 1–12 GHz

centers and micro-capacitor like structures in CPCs. Polarization centers are formed due to the defects in conductive nano fillers while micro-capacitors like structures are formed as a result of the fact that the CNF and TPU act as electrode and dielectric insulator material in the composite structure, respectively [19]. In the micro-capacitor like structures, increasing amount of CNF and SM method led to decrease the thickness of insulating polymer layer between electrode-like CNFs thus electronic polarization of polymer phase can be carried out easily. As seen in Fig. 7, it was obtained that the increasing amount of CNF into composition

or employing of SM method yielded higher ε' values for all series of samples. By regarding of the imaginary part of permittivity (ε") which is a measure of dissipated energy within materials and it is mainly related to conductivity, higher ε" values with the increasing amount of CNF was obviously due to the formation of more conductive pathways into sample.

EMI shielding performance

Frequency dependence of calculated reflection (SE_R) and absorption (SE_A) shielding effectiveness parameters of samples are given in Fig. 8. It should be noted that the multiple reflection contributions (SE_{MR}) were ignored for all samples. Because it was supposed that the re-reflected waves were absorbed within the material as the thickness of shielding materials was larger than the critical thickness value called as "skin depth".

The SE_R and SE_A curves of samples, calculated with the Eqs. 2 and 3, are illustrated in Fig. 8 as a function of frequency. Thickness of shielding material was taken 2 mm in the SE calculation. It should also be noted that the SE_R cannot be calculated mathematically for samples showing a critical conductivity values. Accordingly, reflection contribution to the SE_T was taken into account for only the CNF-20 samples as the SE_R values could not be determined for the CNF-5 and CNF-10 samples.

As seen in Fig. 8, neat TPU was almost transparent against to EMI radiation (SE ≈ 0–2 dB) in entire frequency range and the shielding performance of composites improved by introducing of CNF into composition possibly due to increasing polarization effect. However, increasing amount of filler resulted in an increase in SE values readily. This effect was pronounced for SE_A at high frequency region. This could be attributed to formation of multiple conduction pathways into bulk structure of sample. On the other hand, it was also obtained that the SE_R curves of CNF-20 samples prepared with different routes decreased with the frequency increase. These curves indicate that the contributions of SE_A and SE_R are improtant and they both must be improved at low and high frequency regions to develop effective electromagnetic shielding materials. By considering the microstructural observations and electrical conductivity results of samples, it was found that highly conductive composites prepared with SM method showed higher EMI shielding performance than compositional counterparts due to their higher A_f values and formation of multiple conduction pathways.

Some compositional and electromagnetic properties of various kinds of thermoplastic composites prepared by using different type carbon fillers and processing methods are listed in Table 2. In this table, electrical conductivity and EMI shielding performances of mainly TPU based and a few other elastomeric matrix composites are reported and compared depending on the compositional features and processing methods. As explained in the introduction part, it should be noted again that EMI shielding performances of carbon filled thermoplastic composites depend on many structural, morphological parameters and some external factors such as chemical and physical properties of raw materials, thermomechanical history and processing conditions, dispersion quality of fillers, sample thickness, and experimental errors during measurements etc. We believe that these values could be used to roughly compare the application performances of such systems. Based on the relevant literature reported previously, it can be concluded that EMI shielding effectiveness of carbon filled TPU composites can exceed 20 dB within the frequency range of X and/or Ku band when the amount of filler is above electrical percolation threshold and the sample thickness is higher than 2 mm.

The frequency dependent SE_T curves of CNF-20 samples prepared with different processing routes and in the thickness range of 1–5 mm are given in Fig. 9. Minimum total shielding effectivity requirements for several applications are also specified in these figures. The SE_T curves of MC-20 sample revealed that the level of 20 dB, minimum acceptable shielding value for many applications, cannot be obtained with a 5 mm sample within the frequency range of 1–12 GHz. On the other hand, the SM-U-20 and SM-20 samples having a thickness at least 2 mm provide this shielding level specifically in the X-

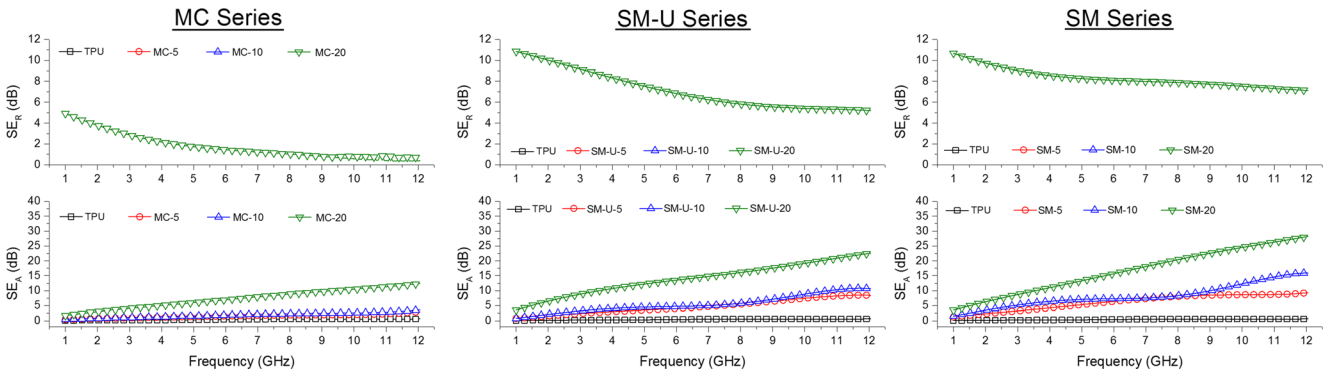

Fig. 8 Dependence of shielding effectiveness of samples on the composition and processing method within the frequency range of 1–12 GHz

Table 2 Sample notation and compositions

Polymer matrix	Filler	Amount of filler (wt%)	Preparation method	Frequency range (GHz)	Sample thickness (mm)	EMI SE (dB)	Conductivity (S/cm)	Ref.
TPU	EG	20	Melt blending	8–12	4	20	n.a.	[12]
TPU	GNP + CNT	10	Solution mixing	12.4–18	3	47	0.095	[28]
TPU	GNS	0.12*	Solution mixing	8–12	0.05	14	~ 0.01	[29]
TPU	TRG	5.5*	Solution mixing	12.4–18	2	26–32	0.00031	[30]
TPU	GNC	25	Paste mixing followed by hot pressing	8–12	2	26.4	0.07288	[31]
TPU	TRG	5.5*	Solution mixing followed by compression molding	8.2–12.4	3	21	~ 0.001	[32]
TPU	CNF	20	Solution mixing	8.2–12.4	3	~ 20	n.a.	[33]
TPU	CB	9.3	Solution mixing	8–18	1.3	18	n.a.	[34]
PU	GNP	6.5*	in-situ polymerization	30 kHz- 3 GHz	1	19.34	0.01	[35]
TPU	MWCNT	10	Solution mixing	8.2–12.4	2.5	41.6	7.9	[36]
CPE	CNF	10	Melt blending Solution mixing subsequent melt blending	8.2–12.4	1	22 24	~ 10^{-6} ~10^{-5}	[37]
PVA	MWCNT	10	Electrospinning	8–12	3	> 40	0.87	[26]
EMA	CB	20	Solution mixing	8.2–12.4	2	33.9	~ 0.01	[27]
PSAN	GFs	7	Hot compression molding	8.5–12.5	1–2	> 41	~ 1	[38]
TPU	CNF	20	Solution mixing	9–12	2	30–40	~ 10	This study
TPU	CNF	20	Solution mixing	7–12	5	55–80	~ 10	This study

TPU Thermoplastic polyurethane, *CPE* Chlorinated polyethylene, *PVA* Polyvinyl alcohol, *EMA* ethylene-methyl acrylate copolymer, *PSAN* poly (styrene-*co*-acrylonitrile)

EG Exfoliated graphite, *GNP* Graphene/graphite nano platelets, *CNT* Carbon nanotube, *GNS* Graphene nanosheets, *GNC* Graphene-like nano carbon sheets, *TRG* Thermally reduced graphene nanosheets, *CNF* Carbon nanofiber, *CB* carbon black, *MWCNT* Multi-walled carbon nanotube, *GFs* Graphite flakes

*volume fraction, *n.a.* not applicable / unreported

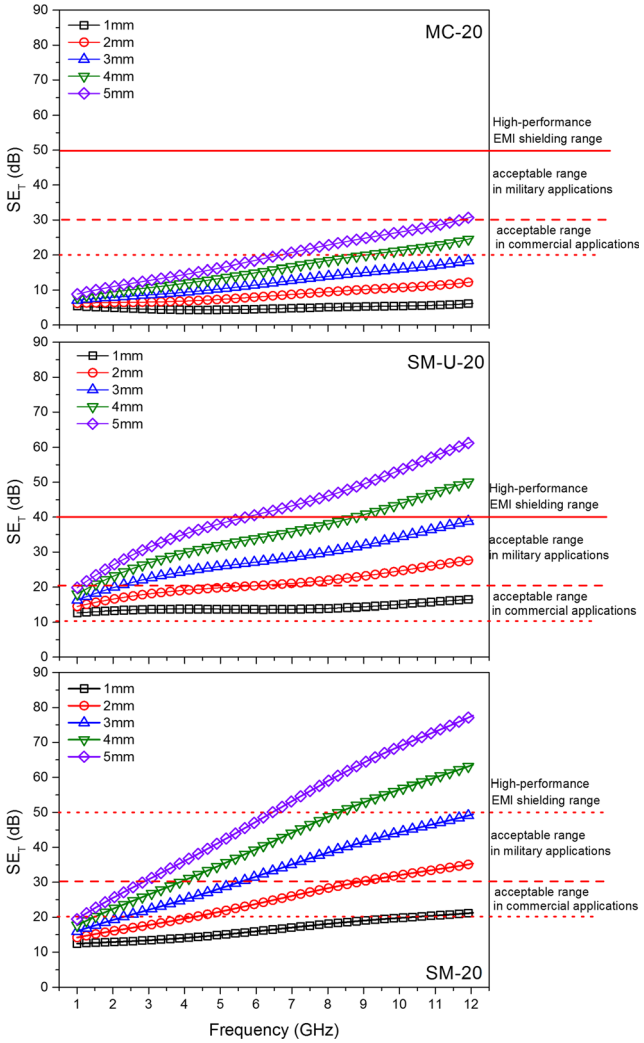

Fig. 9 Dependence of total shielding effectiveness values of samples consisting of 20 phr of CNF on the composite thickness and processing method within the frequency range of 1–12 GHz

band range (8–12 GHz) which is important for military applications.

Conclusion

In this study, effect of composite preparation method on the microstructural features, electrical conductivity and EMI shielding performances of TPU-CNF composites were investigated. It was found that processing route strongly affected to microstructure formation and relevant morphological properties of composite samples such as dispersion and aspect ratio of CNFs, structural and interfacial uniformity, porousity and surface topology etc. It was also suprisingly found that better filler dispersion did not yielded better electrical conductivity and EMI shielding performance for the CNF filled polymer composites. Electromagnetic properties and EMI shielding performances of composites showed that a TPU-CNF composite sheet having a 20 phr of filler, thickness of 2 mm, and prepared with simple solution mixing method can effectively shield an incident electromagnetic wave within the frequency range of 8–12 GHz. If the thickness of composite increases, shielding effectiveness can be improved and high performance, flexible shielding materials can be prepared by using 20 phr of CNF.

Acknowledgements This study was supported by TUBITAK, The Scientific and Technological Research Council of Turkey, with the Project Number of 214 M562.

References

1. Bhargav H, Srinivasan TM, Varambally S, Gangadhar BN, Koka P (2015) Effect of mobile phone-induced electromagnetic field on brain hemodynamics and human stem cell functioning: possible mechanistic link to cancer risk and early diagnostic value of electronphotonic imaging. J Stem Cells 10(4):287
2. Kramarenko AV, Tan U (2003) Effects of high-frequency electromagnetic fields on human EEG: a brain mapping study. Int J Neurosci 113(7):1007–1019
3. Mann K, Röschke J (1996) Effects of pulsed high-frequency electromagnetic fields on human sleep. Neuropsychobiology 33(1):41–47
4. Chen Z, Xu C, Ma C, Ren W, Cheng HM (2013) Lightweight and flexible graphene foam composites for high- performance electromagnetic interference shielding. Adv Mater 25(9):1296–1300
5. Dhakate SR, Subhedar KM, Singh BP (2015) Polymer nanocomposite foam filled with carbon nanomaterials as an efficient electromagnetic interference shielding material. RSC Adv 5(54):43036–43057
6. Messenger GC, Ash MS (1986) The effects of radiation on electronic systems. Van Nostrand Reinhold Co. Inc., New York
7. Chung DDL (2001) Electromagnetic interference shielding effectiveness of carbon materials. Carbon 39(2):279–285
8. Qin F, Brosseau C (2012) A review and analysis of microwave absorption in polymer composites filled with carbonaceous particles. J Appl Phys 111(6):4
9. Al-Saleh MH, Saadeh WH, Sundararaj U (2013) EMI shielding effectiveness of carbon based nanostructured polymeric materials: a comparative study. Carbon 60:146–156
10. Thomassin JM, Jérôme C, Pardoen T, Bailly C, Huynen I, Detrembleur C (2013) Polymer/carbon based composites as electromagnetic interference (EMI) shielding materials. Mater Sci Eng R Rep 74(7):211–232
11. Mishra M, Singh AP, Dhawan SK (2013) Expanded graphite–nanoferrite–fly ash composites for shielding of electromagnetic pollution. J Alloys Compd 557:244–251
12. Valentini M, Piana F, Pionteck J, Lamastra FR, Nanni F (2015) Electromagnetic properties and performance of exfoliated graphite (EG)–Thermoplastic polyurethane (TPU) nanocomposites at microwaves. Compos Sci Technol 114:26–33
13. Liu Y, Song D, Wu C, Leng J (2014) EMI shielding performance of nanocomposites with MWCNTs, nanosized Fe_3O_4 and Fe. Compos Part B 63:34–40
14. Yuan B, Yu L, Sheng L, An K, Zhao X (2012) Comparison of electromagnetic interference shielding properties between single-wall carbon nanotube and graphene sheet/polyaniline composites. J Phys D Appl Phys 45(23):235108

15. Shen B, Zhai W, Zheng W (2014) Ultrathin flexible graphene film: an excellent thermal conducting material with efficient EMI shielding. Adv Funct Mater 24(28):4542–4548
16. Kuzhir P, Paddubskaya A, Plyushch A, Volynets N, Maksimenko S, Macutkevic J, Celzard A (2013) Epoxy composites filled with high surface area-carbon fillers: optimization of electromagnetic shielding, electrical, mechanical, and thermal properties. J Appl Phys 114(16):164304
17. Singh BP, Saini K, Choudhary V, Teotia S, Pande S, Saini P, Mathur RB (2014) Effect of length of carbon nanotubes on electromagnetic interference shielding and mechanical properties of their reinforced epoxy composites. J Nanopart Res 16(1):2161
18. Verma P, Saini P, Choudhary V (2015) Designing of carbon nanotube/polymer composites using melt recirculation approach: effect of aspect ratio on mechanical, electrical and EMI shielding response. Mater Des 88:269–277
19. Arjmand M, Apperley T, Okoniewski M, Sundararaj U (2012) Comparative study of electromagnetic interference shielding properties of injection molded versus compression molded multi-walled carbon nanotube/polystyrene composites. Carbon 50(14):5126–5134
20. Yang RB, Kuo WS, Lai HC (2014) Effect of carbon nanotube dispersion on the complex permittivity and absorption of nanocomposites in 2–18 GHz ranges. J Appl Polym Sci 131(21)
21. Saini P, Arora M, Gupta G, Gupta BK, Singh VN, Choudhary V (2013) High permittivity polyaniline–barium titanate nanocomposites with excellent electromagnetic interference shielding response. Nanoscale 5(10):4330–4336
22. Geetha S, Satheesh Kumar KK, Rao CR, Vijayan M, Trivedi DC (2009) EMI shielding: methods and materials-a review. J Appl Polym Sci 112(4):2073–2086
23. Sambyal P, Singh AP, Verma M, Farukh M, Singh BP, Dhawan SK (2014) Tailored polyaniline/barium strontium titanate/expanded graphite multiphase composite for efficient radar absorption. RSC Adv 4(24):12614–12624
24. Kumar GS, Vishnupriya D, Joshi A, Datar S, Patro TU (2015) Electromagnetic interference shielding in 1–18 GHz frequency and electrical property correlations in poly (vinylidene fluoride)–multi-walled carbon nanotube composites. Phys Chem Chem Phys 17(31):20347–20360
25. Al-Saleh MH, Sundararaj U (2009) Electromagnetic interference shielding mechanisms of CNT/polymer composites. Carbon 47(7):1738–1746
26. Nasouri K, Shoushtari AM (2017) Designing, modeling and manufacturing of lightweight carbon nanotubes/polymer composite nanofibers for electromagnetic interference shielding application. Compos Sci Technol 145:46–54
27. Mondal S, Ganguly S, Das P, Khastgir D, Ch Das N (2017) Low percolation threshold and electromagnetic shielding effectiveness of nano-structured carbon based ethylene methyl acrylate nanocomposites. Compos Part B 119:41–56
28. Verma M, Chauhan SS, Dhawan SK, Choudhary V (2017) Graphene nanoplatelets/carbon nanotubes/polyurethane composites as efficient shield against electromagnetic polluting radiations. Compos Part B 120:118–127
29. Jan R, Habib A, Akram MA, Ahmad I, Shah A, Sadiq M, Hussain A (2017) Flexible, thin films of graphene–polymer composites for EMI shielding. Mater Res Express 4:035605
30. Bansala T, Joshi M, Mukhopadhyay S, Doong R, Chaudhary M (2017) Electrically conducting graphene-based polyurethane nanocomposites for microwave shielding applications in the Ku band. J Mater Sci 52:1546–1560
31. Kumar A, Alegaonkar PS (2015) Impressive transmission mode electromagnetic interference shielding parameters of graphene-like nanocarbon/polyurethane nanocomposites for short range tracking countermeasures. ACS Appl Mater Interfaces 7:14833–14842
32. Verma M, Verma P, Dhawan SK, Choudhary V (2015) Tailored graphene based polyurethane composites for efficient electrostatic dissipation and electromagnetic interference shielding applications. RSC Adv 5:97349–97358
33. Durmus Z, Durmus A, Bektay MY, Kavas H, Unver IS, Aktas B (2016) Quantifying structural and electromagnetic interference (EMI) shielding properties of thermoplastic polyurethane–carbon nanofiber/magnetite nanocomposites. J Mater Sci 51:8005–8017
34. Gupta KK, Abbas SM, Abhyankar AC (2016) Carbon black/polyurethane nanocomposite-coated fabric for microwave attenuation in X & Ku-band (8–18 GHz) frequency range. J Ind Text 46(2):510–529
35. Puri P, Mehta R, Rattan S (2015) Synthesis of conductive polyurethane/graphite composites for electromagnetic interference shielding. J Electron Mater 44(11):4255–4268
36. Gupta TK, Singh BP, Teotia S, Katyal V, Dhakate SR, Mathur RB (2013) Designing of multiwalled carbon nanotubes reinforced polyurethane composites as electromagnetic interference shielding materials. J Polym Res 20:169
37. Mondal S, Nayak L, Rahaman M, Aldalbahi A, Chaki TK, Khastgir D, Ch Das N (2017) An effective strategy to enhance mechanical, electrical, and electromagnetic shielding effectiveness of chlorinated polyethylene-carbon nanofiber nanocomposites. Compos Part B 109:155–169
38. Panwar V, Gill FS, Rathi V, Tewari VK, Mehra RM, Park J-O, Park S (2017) Fabrication of conducting composite sheets using cost-effective graphite flakes and amorphous styrene acrylonitrile for enhanced thermistor, dielectric, and electromagnetic interference shielding properties. Mater Chem Phys 193:329–338